Kinetic Characterization of the pH-Dependent Oligomerization of R67 Dihydrofolate Reductase†

Annick Méjean,* Christophe Bodenreider, Katja Schuerer, and Michel E. Goldberg

Unité de Biochimie Cellulaire, CNRS URA 2185, Institut Pasteur, 28 rue du Dr. Roux, 75724 Paris Cédex 15, France

Received March 27, 2001; Revised Manuscript Received May 10, 2001

ABSTRACT: Protein−protein recognition results from the assembly of complementary surfaces on two molecules that form a stable, noncovalent, specific complex. Our interest was to describe kinetic aspects of the recognition in order to understand the subtle molecular mechanism of association. R67 dihydrofolate reductase (DHFR) provides an ideal model to investigate kinetic parameters of protein−protein association since it is a homotetramer resulting from the pH-dependent dimerization of homodimers. We took advantage of the presence of a tryptophan residue at the dimer−dimer interface to monitor pH-dependent oligomerization of R67 DHFR using stopped-flow fluorescence techniques. Except for pH near neutrality where dissociation exhibited biphasic kinetics, association and dissociation followed monophasic kinetics fitted on a two-state model. Apparent rate constants of association k_{on} and dissociation k_{off} were determined at various pHs and pointed to the key role of a histidine located at the dimer−dimer interface in the pH control of tetramerization. The values of the tetramer−dimer equilibrium dissociation constant were calculated from the ratio k_{off}/k_{on} and correlated well with those previously measured at equilibrium. The thermodynamic parameters and the activation energies of both the association and dissociation were determined and indicated that the association is enthalpy driven and suggested that the formation of four hydrogen bonds (one per monomer) is responsible for the thermodynamic stability of the tetramer. Detailed analysis of the biphasic kinetics led to an original model, in which protonation of the tetramer is the triggering event for the dissociation process while the association involves primarily the unprotonated dimers.

Many biological processes are carried out or regulated through interactions between proteins. The importance of such interactions in biology has made the protein−protein recognition process an area of considerable interest and has been extensively studied (*1*−*3*). However, most studies have been carried out at equilibrium, because a variety of sensitive and accurate experimental methods can be easily used to measure equilibrium constants and, hence, determine free energies of association. Moreover, the increased sensitivity and precision of the new generations of microcalorimeters enable one to obtain a complete thermodynamic description of the association−dissociation through the simultaneous determination of the free energy, enthalpy, and entropy associated with the interaction. Such studies have been conducted in parallel with the determination of the 3D structure of the isolated and associated proteins and with the use of site-directed mutagenesis. Examples of systems that have been most extensively studied along these lines are the complex formed between hen lysozyme and the Fab fragment derived from the specific monoclonal antibody D1.3 (*4*−*9*) and the association of barnase with its intracellular inhibitor barstar (*10*−*13*). This approach has opened the way to a detailed understanding of the role of individual amino acid side chains in building up stable and specific interactions.

Despite these impressive advances, our understanding of protein−protein interactions is far from being complete. In particular, modeling of the interaction energies based on the 3D structures is still not practicable to reliably predict the effects of mutations on the stability of a protein−protein interaction nor even of a protein−ligand interaction in the case of a small ligand. Yet, such predictions are of utmost importance in the design of molecules (agonists or antagonists) of therapeutic interest. Similarly, the kinetic aspects of protein−protein interactions have rarely been investigated in depth, despite their essential role in the control of some biological processes and of the information they can provide on the molecular mechanisms of the association−dissociation process. It therefore appeared of interest to undertake, on a unique molecular system, a complete set of investigations encompassing the energetic, kinetic, and modeling aspects of protein−protein interaction. The present work was aimed at providing a dynamic vision of the interactions involved in the association−dissociation process as part of a comprehensive theoretical model of protein−protein interactions that our laboratory attempts to develop (*14*).

The model system we have chosen for that purpose is the dihydrofolate reductase encoded by the plasmid R67 of *Escherichia coli* (R67 DHFR).[1] This protein (*15*, *16*) is interesting for several reasons. At pHs above neutrality, it is a stable homotetramer (MW 33 720). It, however, under-

† This work was supported by funds from the Institut Pasteur and the Centre National de la Recherche Scientifique (URA 2185). C.B. was supported by a fellowship from the Ministère de l'Education Nationale de la Recherche et de la Technologie.

* Corresponding author. Tel: 33 1 40 61 32 81. Fax: 33 1 40 61 30 43. Email: amejean@pasteur.fr.

10.1021/bi010611j CCC: $20.00
Published on Web 06/13/2001

goes a pH-dependent equilibrium, with a stable dimeric form below pH about 5.0 (*17*). The crystal structures of the dimer and tetramer have been solved (*18*, *19*). R67 DHFR is one of the smallest monomers (78 residues) (*20*) known to assemble into a catalytically active protein. Though it catalyzes the same reaction as chromosomal DHFRs, it has, interestingly, no sequence or structural homology with the chromosomal enzyme (*21*). Its activity is responsible for the resistance to the antibiotic trimethoprim (*15*, *20*, *21*). The R67 DHFR is active in the tetrameric state (*17*). It catalyzes the NADPH-dependent reduction of 7,8-dihydrofolate (DHF) into 5,6,7,8-tetrahydofolate (THF) in a single active site pore, passing through the middle of the doughnut-shaped macromolecule (*22*, *23*). Each subunit has a core structure consisting of five antiparallel β-strands that form in the dimer a compact intersubunit β-barrel (*19*). The monomer is not stable as an isolated species as shown by denaturation equilibrium studies (*24*, *25*). Dimeric R67 DHFR is stable at acidic pH (pH 5.0) but inactive or weakly active (*17*). Two dimers associate, when the pH is increased to pH 8.0 or above, to form a stable active tetramer (*17*). The crystal structure shows that each dimer−dimer interface is stabilized by a hydrogen bond formed between the imidazole ring of the histidine 62 from one protomer and the hydroxyl group of the nearby serine 59 from the symmetry-related protomer (*19*). Hydrogen bonds are very often involved in determining binding specificity, and the effects of point mutations at these two positions in R67 DHFR have confirmed the importance of the hydrogen bond between Ser 59 and His 62 (*14*, *26*). Some 14 mutants affected at one position only were constructed (*14*), and all were shown to be dimers even at pH 8.0. However, several pairs of protein variants, each bearing a single point mutation, one at position 59 and the other at position 62, were shown to form active heterotetramers in which two hydrogen bonds (out of the four initially present in the wild-type enzyme) suffice to stabilize the tetrameric form at alkaline pH. In particular, the variants S59A and H62L were shown to spontaneously assemble into a stable heterotetramer with catalytic properties close to those of the wild-type protein but with a less pronounced pH dependence of the association. The double mutant (S59A, H62L) was also constructed. It formed an active homotetramer which, interestingly, showed no pH dependence of its oligomeric state. Clearly, these two mutations compensate each other, presumably by creating a type of interaction that replaces the lost hydrogen bond. These observations directly point to the role of the hydrogen bond between S59 and H62 in the control of the pH-dependent tetramer−dimer equilibrium in R67 DHFR.

As a complement to these studies at equilibrium and by computer modeling, the present report focuses on the kinetic aspects of the association and dissociation reactions involved in the R67 DHFR dimer−tetramer equilibrium. The aim of the kinetic approach was to evaluate the adequacy of the molecular mechanisms underlying the models used to interpret the experimental equilibrium data and to design the modeling algorithm (*27*). Indeed, the modeling studies referred to in the previous section rely on the assumption that the equilibrium obeys a simple two-states mechanism described by the reaction scheme:

$$T \underset{k_{on}}{\overset{k_{off}}{\rightleftharpoons}} 2D$$

where D and T represent the unprotonated (on His 62) dimeric and tetrameric forms, respectively, of the molecule. Similarly, the determination of the equilibrium constants from the experimental data involved the same model, since the experimental method used to monitor the oligomerization state distinguishes only two types of molecules: the dimers and the tetramers. This probably results in erroneous estimates of the intrinsic constant of the oligomerization equilibrium, since protonated as well as unprotonated dimers must coexist in significant amounts at pHs below neutrality. Indeed, previously reported equilibrium studies (*17*, *28*, *29*) led to the conclusion that the pH controls the overall equilibrium by changing the protonation state of the dimers, according to the scheme:

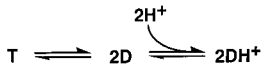

To ascertain the validity of these simple models and to gain a better insight into the molecular mechanisms involved in the dimer−dimer interaction, stopped-flow methods were applied to dimeric or tetrameric R67 DHFR to monitor, via changes in its fluorescence properties, the kinetics of association or dissociation triggered by pH jumps. Such experiments performed at different pHs and temperatures will be reported. The association and dissociation rate constants obtained, for final pHs below 6.5, by fitting the experimental data to a simple two-states model will be reported. The free energies, enthalpies, entropies, and activation energies of dissociation derived from these rate constants will be discussed. The biphasic kinetics observed for the dissociation at pHs above 6.5 will be discussed in terms of a more complex model, which accounts for the pH dependence of the association−dissociation reaction not only in terms of equilibrium but also in terms of kinetics.

MATERIALS AND METHODS

Plasmid Construction. Mutants and wt R67 *dhfr* genes (*30*) subcloned in the expression vector pET19b (Novagen) were a gift of J. Dam and Dr. T. Rose. BLi5 bacteria (corresponding to BL21 lacIQpACYC Cm^R derived from Novagen) were transformed with the corresponding plasmid.

Expression and Protein Purification. E. coli cells were grown in Luria−Beriani (LB) medium in the presence of 0.1 mg/mL ampicillin and 0.03 mg/mL chloramphenicol at 37 °C, and R67 DHFR expression was induced by IPTG (1 mM) when the turbidity of the culture reached $OD_{600} = 0.7$. Cells were collected at stationary phase, centrifuged for 15 min at 1000*g* and 4 °C, and sonicated. Cell debris was removed by centrifugation, and the supernatant was titrated to pH 3.5 by addition of 1 M HCl. Precipitated material was removed by centrifugation, and the supernatant was neutralized to pH 8.0. Protein was then concentrated by 85%

[1] Abbreviations: DHFR, dihydrofolate reductase; MTA buffer, 50 MES, 100 mM Tris, and 50 mM acetic acid polybuffer; T, tetramer; D, dimer; DH^+_n, protonated dimer; TH^+_n, protonated tetramer. Mutant enzymes containing amino acid substitutions are described by the wild-type residue and numbered position in the sequence, followed by the amino acid substitution. For example, S59A R67 DHFR describes the Ser 59→Ala mutant.

ammonium sulfate precipitation. After dialysis, the protein solution was applied to a 4.6 × 100 mm POROS 20HQ column (Boehringer) equilibrated in 10 mM Tris-HCl, pH 8.0, and eluted at a flow rate of 2 mL/min with a linear gradient from 0 to 0.5 M NaCl in10 mM Tris-HCl, pH 8.0. R67 DHFR eluted at approximately 0.15 M NaCl. Protein fractions were checked for purity on SDS−PAGE (*31*), then pooled, dialyzed against 0.5% NH_4HCO_3, lyophilized, and stored at −20 °C. Protein concentration was routinely measured using an extinction coefficient of 1.825 mL·mg^{-1}·cm^{-1} at 280 nm (*24*).

Enzyme Assay. Dihydrofolate reductase activity was assayed as described by Smith and Burchall (*48*) at 30 °C in a 50 mM potassium phosphate, pH 7.0, buffer containing 1 mM DTT, 50 μM NADPH, and 50 μM DHF. One enzyme unit was defined as the amount of enzyme required to reduced 1 mmol of dihydrofolate/min, based on a molar extinction coefficient of 12 300 L·cm^{-1}·mol^{-1} (*32*). We verified that the purified wt R67 DHFR had a specific activity equivalent to protein purified using other procedures (*33*).

Fluorescence Spectra and Buffering System. The protein fluorescence emission spectrum was monitored at 20 °C in an LS5B (Perkin-Elmer) spectrofluorometer in 50 mM MES, 100 mM Tris-HCl, and 50 mM acetic acid buffer (MTA) adjusted to pH 5.0 or 8.0 with 1 N HCl and 5 N NaOH. This buffering system is particularly adapted for studying pH-dependent processes since it maintains a constant ionic strength over the pH range 4.5−9.5 without any change in the concentration of each constituent (*34*). A standard curve pH = f(% MTA buffer, pH 8.0) was constructed for each studied temperature in order to determine the precise stoechiometry between the MTA buffer, pH 5.0, and the MTA buffer, pH 8.0, required to obtain the exact pH within ±0.1 in the pH range 5.0−8.0. Since the pH varies with temperature, standard curves had to be made for each desired temperature. The protein concentration was 20 μg/mL. The excitation and emission bandwidths were 5 nm, and the scan speed was 30 nm/min.

Stopped-Flow Measurements. All of the kinetic experiments were carried out with an SFM3 mixing device from Bio-Logic (Pont de Claix, France) equipped with two large (18 mL) syringes injecting into the first mixer and a small syringe (5 mL) injecting into the second mixer. The mixing device, equipped with an F15 (1.5 mm × 1.5 mm cross section) fluorescence cell, was combined with the optical bench and detection module of Bio-Logic. Two photomultipliers were used, one for the detection of the emitted light through a 350 nm high-pass filter and the second for the detection of the excitation light. The ratio of the two signals was electronically determined in the Bio-Logic dual amplifier, recorded, and analyzed by means of the Bio-Kine software package of Bio-Logic. In all experiments, reaction was initiated in 60 ms by a pH jump from pH 8.0 (for dissociation) or 5.0 (for association) to the designed final pH, mixing 20 μL (from the small syringe) of 400 μg/mL protein with 380 μL of a mix of MTA buffer, pH 8.0 (from one large syringe), and MTA buffer, pH 5.0 (from the second large syringe), in proportions required to obtain the desired final pH. The resulting flow rate corresponded to a dead time of 5.5 ms. The pH of the mix at the desired temperature was verified at the outlet of the cell. The stopped-flow temperature was controlled by means of an external thermostated water bath and a high-flux pump to circulate the water between the bath and the stopped-flow apparatus. The standard temperature was 20 °C. For continuous-flow experiments, the volumes injected and the duration of the injections will be described for each experiment.

Data Analysis. For each set of experimental conditions, 10−30 kinetic traces were obtained, and the accumulated kinetic data were averaged and converted into an ASCII file. The resulting file was analyzed with the Figure P program (version 2.7 for Windows, Biosoft, Cambridge, U.K.) assuming a two-state mechanism of oligomerization:

$$\mathrm{T} \underset{k_{on}}{\overset{k_{off}}{\rightleftharpoons}} 2\mathrm{D}$$

where T is the tetrameric form and D is the dimeric form of R67 DHFR and k_{on} and k_{off} are the rate constants of association and dissociation, respectively. The appearance of the dimeric form can be described by

$$\frac{\mathrm{d[D]}}{\mathrm{d}t} = 2k_{off}[\mathrm{T}] - 2k_{on}[\mathrm{D}]^2 \qquad (1)$$

If C_t represents the total molarity of monomer, $C_t = 4[\mathrm{T}] + 2[\mathrm{D}]$, then the appearance of the dimer can be described by

$$\frac{\mathrm{d[D]}}{\mathrm{d}t} = \frac{k_{off}C_t}{2} - k_{off}[\mathrm{D}] - 2k_{on}[\mathrm{D}]^2 \qquad (2)$$

After resolution of the polynomial and integration, the dimer concentration can be expressed as a function of time, with $[\mathrm{D}] = [\mathrm{D}_0]$ at time 0, as

$$[\mathrm{D}] = \frac{r_1([\mathrm{D}_0] - r_1) - r_2([\mathrm{D}_0] - r_1)\mathrm{e}^{-zt}}{[\mathrm{D}_0] - r_2 - ([\mathrm{D}_0] - r_1)\mathrm{e}^{-zt}} \qquad (3)$$

where

$$z = \sqrt{k_{off}{}^2 + 4k_{off}k_{on}C_t}$$

$$r_1 = \frac{-k_{off} + z}{4k_{on}}$$

$$r_2 = \frac{-k_{off} - z}{4k_{on}}$$

The time course of the fluorescence change was described by the equation:

$$F(t) = F_D[\mathrm{D}] + F_T[\mathrm{T}] \qquad (4)$$

where $F(t)$ is the total amplitude at time t, F_D and F_T are the specific fluorescences of the dimer and the tetramer, respectively, and [D] and [T] the concentrations of dimer and tetramer at time t. After substitution of [T] by its expression as a function of C_t

$$F(t) = \left(F_D - \frac{F_T}{2}\right)[\mathrm{D}] + C_t\frac{F_T}{4} \qquad (5)$$

The above equation was combined with eq 3 into a single equation where the fluorescence is expressed as a function of time as

$$F(t) = \left(F_D - \frac{F_T}{2}\right)\frac{r_1([D_0] - r_1) - r_2([D_0] - r_1)e^{-zt}}{[D_0] - r_2 - ([D_0] - r_1)e^{-zt}} + C_t\frac{F_T}{4} \quad (6)$$

with C_t and $[D_0]$ fixed. $[D_0]$ is calculated from the C_t value considering that all of the protein population is dimeric at pH 5.0 whereas at pH 8.0 the dimer fraction represents 15% of the total protein concentration where $C_t = 2.4$ μM (*17*). Using the nonlinear least-squares curve fitter provided by the Figure P program, experimental data were fitted to eq 6 using fixed values for C_t and $[D_0]$ (see above). These fittings provided estimates of k_{on} and k_{off} simultaneously.

RESULTS

Association Dependence of the R67 DHFR Fluorescence. R67 DHFR contains two tryptophans per monomer, one (W45) located at the monomer−monomer interface and the other (W38) at the dimer−dimer interface in the tetrameric protein (*18*, *19*, *24*). Figure 1 shows the fluorescence emission spectra of the protein at pH 5.0, where it is essentially dimeric, and at pH 8.0, where it is mostly tetrameric. As previously described (*17*), the transition of W38 from a hydrophobic (in the tetramer) to hydrophilic (in the dimer) environment results in a red shift of the emission spectrum (excitation at 295 nm), with a maximum at 340 nm for the dimer as compared to 330 nm for the tetramer. The tetramer specific fluorescence was calculated by integrating the area spectrum from 340 to 400 nm and is about 60% that of the dimer. This large change in protein fluorescence was used to monitor the pH dependence of oligomerization of R67 DHFR in stopped-flow experiments.

Fluorescence Stopped-Flow Experiments. Figure 2 displays representative examples of dissociation (A) and association (B) stopped-flow traces observed during 100 s after jumps from pH 8.0 (A) or pH 5.0 (B) to pH 6.2 in the final mix. The pH increase resulted in a fluorescence decrease, consistent with the appearance of tetramers, whereas the pH decrease resulted in a fluorescence increase corresponding to an enrichment in the dimer population. The association kinetics reached a plateau after 60 s, while the dissociation kinetics were slower. The kinetic traces were processed using nonlinear least-squares fitting of eq 6 which expresses the dimer concentration as a function of time according to a reversible two-state model. This procedure provided good fits of the fluorescence traces, with low values for the sum of the residuals squared (X^2 of the order of 0.01) and random distribution of the residuals, and allowed to estimate both the association and the dissociation rate constants. Thus, analysis of the traces of Figure 2 provided the association rate constant $k_{on} = 7600 \pm 166$ $M^{-1}\cdot s^{-1}$ and the dissociation rate constant $k_{off} = 18 \times 10^{-3} \pm 4 \times 10^{-3}$ s^{-1} for pH 6.2 and 20 °C.

Effect of the pH on the Association−Dissociation Kinetics. The pH dependence of the association and dissociation rate constants was studied at 20 °C between pH 5.4 and pH 8.0. Throughout this pH range, the observed kinetics could be satisfactorily fitted using a reversible two-state model (eq 6). However, a reliable estimate of the rate constants could be obtained simultaneously for both the association and the dissociation only for final pHs ranging between 6.1 and 6.9. Below pH 6.1, only the dissociation rate constant could be reliably determined using a downward pH jump, while above pH 6.9, only the association rate constant could be measured with good confidence using an upward pH jump. The pH dependence of the values thus obtained is represented in Figure 3. The association rate constant (Figure 3A) increased slightly (30-fold) between pH 6.0 and pH 8.0 whereas the dissociation rate constant (Figure 3B) decreased almost 200-fold when the pH was increased by less than half a pH unit. A maximum dissociation rate constant of 0.5 s^{-1} was obtained at pH 5.4, and the association rate constant reached a value of 40 000 $M^{-1}\cdot s^{-1}$ at pH 8.0. Interestingly, the half-variation of the pH dependence of the association rate constant corresponded to a pH value of 7.0 while the pK_a of His 62 in the dimeric form of R67 DHFR has been estimated to be 6.8 by proton NMR (*17*). The similarity of these two values supports the idea that His 62 may play a key role in the association process. Despite the restricted range where the pH dependence of the dissociation rate constant could be observed, the apparent half-variation clearly corresponded to a more acidic pH (around 5.5) than that found for the association. This value does not correspond to the classical pK_a of the Nϵ of a histidine but could represent the pK_a of an ionizable residue such as a histidine buried inside the tetramer. Thus, it has been observed in various proteins (*35*−*37*) that the pK_a of a buried histidine is more than one pH unit lower than that of an exposed histidine. It is noteworthy that Howell and collaborators investigated the pH-dependent protein fluorescence at equilibrium for wild-type R67 DHFR, "double" R67 DHFR where the gene had been duplicated and fused (*39*), and "quadruple" R67 DHFR where the gene had been quadruplicated and fused (*28*), resulting respectively in two or four covalently linked original protomers. They showed that the curves are superimposable for the native and double proteins while the pK_a for the quadruple protein was decreased to 5.50 as compared to 6.84 for the wild-type and double proteins. The authors proposed that, since the equilibrium occurred in an intramolecular reaction for the quadruple protein instead of an intermolecular reaction

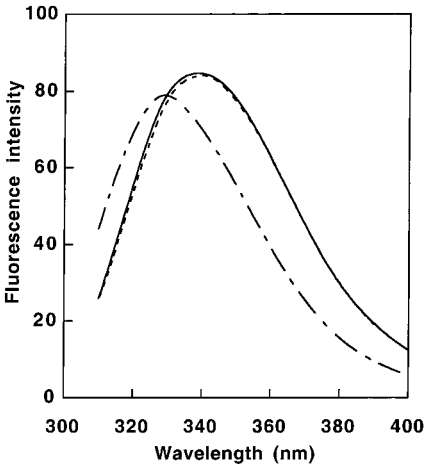

FIGURE 1: Fluorescence emission spectra (excitation at 295 nm) of R67 DHFR wt and the S59A mutant. The wt R67 DHFR (20 mM) spectra are described in solid lines (—) at pH 5.0 and by (— · —) at pH 8.0, whereas the S59A spectra are shown at pH 8.0 and pH 5.0 (indistinguishable spectra) by the dotted line.

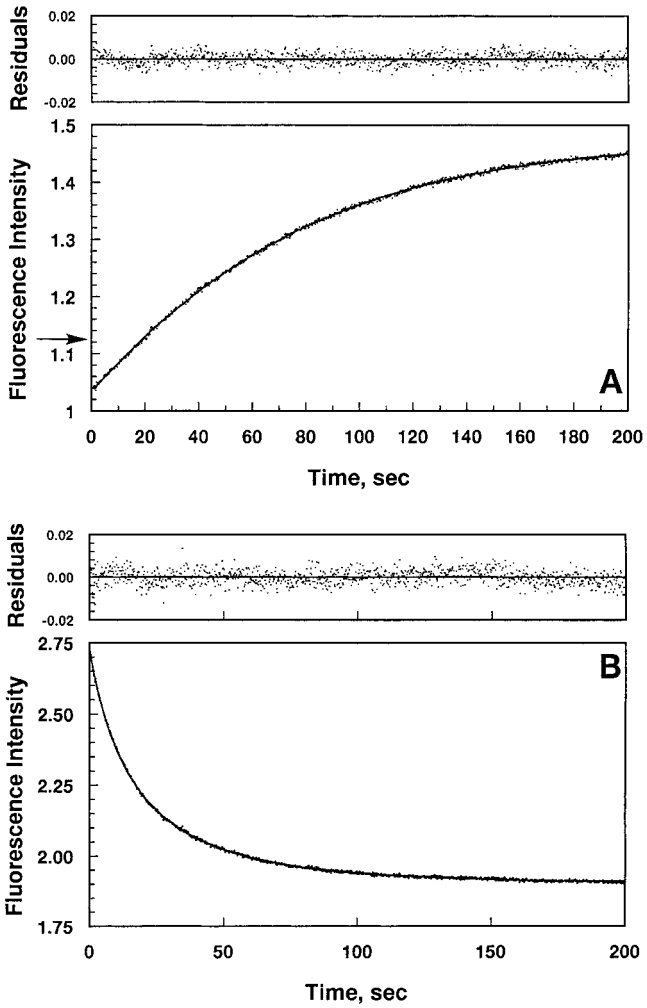

FIGURE 2: Examples of fluorescence stopped-flow experiments. Each trace results from the average of 10 recordings. The solid lines represent the best fits to the experimental points according to eq 6 described in Material and Methods, and the residuals of the fits are shown above each panel. Panel A shows a typical dissociation kinetic after a pH jump from 8.0 to 6.2, and panel B shows association kinetic from pH 5.0 to 6.2. The horizontal arrow, in panel A, indicates the initial value of the fluorescence intensity of the protein at pH 8.0, obtained by injection of 20 μL of 400 μg/mL protein at pH 8.0 with 380 μL of MTA buffer, pH 8.0. The meaning of the arrow will be addressed in Results. The fluorescence intensity is in volts.

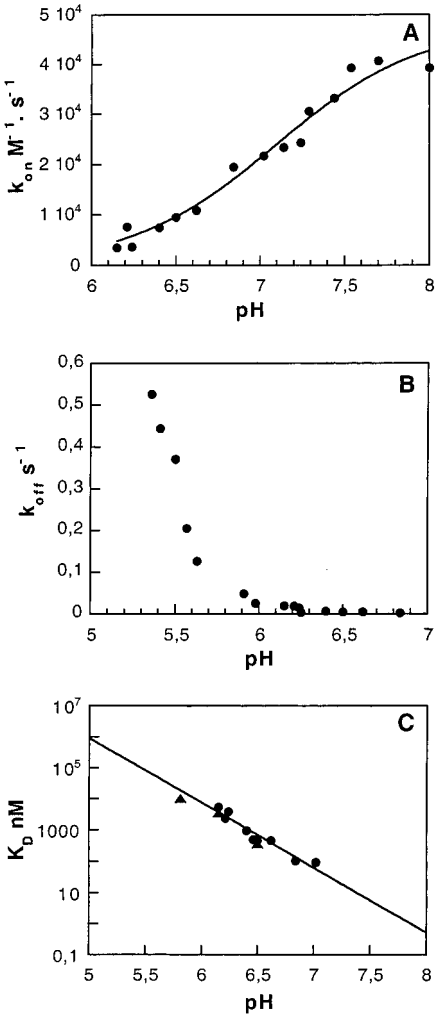

FIGURE 3: Dependence of the association and dissociation rate and equilibrium constants with the pH. The association rate constant k_{on} ($M^{-1}\cdot s^{-1}$) and dissociation rate constant k_{off} (s^{-1}) are plotted against pH on panels A and B, respectively. In panel A, the solid line represents the best fit to the experimental points according to eq 10 (see Discussion). Panel C describes the pH dependence of the equilibrium dissociation constant. The K_D values calculated from the ratio k_{off}/k_{on} are represented as (●) and the K_D values previously determined at equilibrium (*17*) as (▲). A linear correlation between log K_D and pH is obtained and allows to extrapolate the K_D values at the extreme pHs: K_D (pH 5.0) = 0.9 mM and K_D (pH 8.0) = 0.5 nM.

for the wild-type and double proteins, the effective concentration of the associating domains was greatly increased.

The ratios k_{off}/k_{on} in the pH range of 5.8−6.9 were calculated and are shown in Figure 3C. These values are in good agreement with the K_D previously determined at equilibrium using NMR or sedimentation-diffusion experiments (*17*). This indicates that a simple two-state association−dissociation model is appropriate to describe the equilibrium in this pH range. K_D varies 100-fold between pH 6.0 and 7.0. This large variation of the K_D value for only one pH unit primarily reflects the large variation of the dissociation rate constant in this pH range, indicating that the major contribution to the pH sensitivity of the oligomerization equilibrium comes from the dissociation rate constant.

Thermodynamic Parameters and Activation Energies of the Association and Dissociation Reactions. By repeating pH jump experiments at different temperatures ranging between 12 and 32 °C at two pHs (6.5 and 6.8), one could determine the rate constants of association and dissociation as a function of temperature. These rate constants shown in an Arrhenius representation (Figure 4) provided access to the thermodynamic parameters (see Table 1) that govern the association−dissociation equilibrium and kinetics (free energy $\Delta G°$, enthalpy $\Delta H°$, entropy $\Delta S°$, activation energies). Thus, the free energies of dissociation at 20 °C and pH 6.5 and 6.8 were calculated from the ratios k_{on}/k_{off} on the basis of the reaction rate theory. As the pH rose from 5.0 to 8.0, K_D decreased and the dissociation free energy increased since the tetramer population increased. Interestingly, raising the pH from 5.0 to 8.0 caused a free energy change $\Delta\Delta G° = \Delta G°_{pH8} - \Delta G°_{pH5}$ of 8.4 kcal·mol^{-1} for the dissociation of the tetramer into dimers. If one hydrogen bond is assumed to contribute a plausible value of about 2−3 kcal·mol^{-1} (*40*) to the binding free energy, the pH-induced dissociation free energy change estimated above could well correspond to the

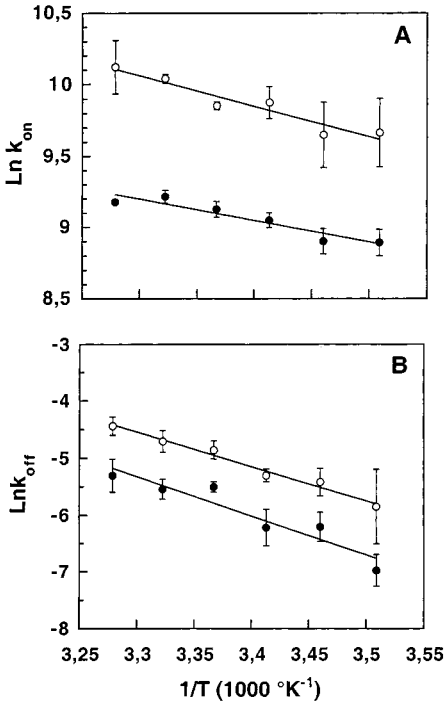

FIGURE 4: Temperature dependence of the association (panel A) and dissociation rate constants (panel B). Rate constants determined at pH 6.5 (●) and at pH 6.8 (○) are represented against the reciprocal of the temperature, expressed in K^{-1}. Each error bar represents the standard deviation determined from at least three independent experiments.

Table 1: Thermodynamic Parameters and Activation Energies for Association and Dissociation Reactions at 20 °C[a]

pH	$\Delta G°$ [b] (kcal/mol)	$\Delta H°$ [c] (kcal/mol)	$\Delta S°$ [d] (cal·mol^{-1}·K^{-1})	E_a(assoc) (kcal/mol)	E_a(dissoc) (kcal/mol)
5.0	4.1				
6.5	8.5	8.0	−1.5	3.0	11.9
6.8	9.4	10.0	+2.1	4.1	13.9
8.0	12.5				

[a] All values are calculated per mole of dimer. [b] $\Delta G°$ is calculated from the relation $\Delta G° = -RT \ln K_D$, where K_D is the ratio k_{off}/k_{on}. For pH 5.0 and 8.0, $\Delta G°$ values are calculated using the K_D values extrapolated from the pH dependence of K_D (Figure 3C). [c] $\Delta H°$ is determined at pH 6.5 and 6.8 from the van't Hoff plot $\ln K_D = f(1/T)$, where the slope yields $\Delta H°/R$ with $R = 2$ cal·mol^{-1}·K^{-1}. [d] $\Delta S°$ is calculated from the values of $\Delta H°$ and $\Delta G°$ by means of equation $\Delta G° = \Delta H° - T\Delta S°$.

establishment of four hydrogen bonds per tetramer when the pH is raised from 5.0 to 8.0.

Activation energies (E_a) for both the association and the dissociation reactions were estimated from the slope of the straight lines obtained in the corresponding Arrhenius plots (Figure 4). The free energy differences between the transition state and the dimer [E_a(association)] or the tetramer [E_a(dissociation)] thus obtained are reported in Table 1. Like for the pH effect, the temperature dependence was significantly more pronounced for the dissociation than for the association rate constant. The strong increase (5-fold) of the dissociation rate with temperature may reflect an increased protein "breathing" facilitating the proton accessibility to the dimer−dimer interface. Indeed, E_a(association) is about 3−4-fold smaller than E_a(dissociation), indicating that the energy barrier is higher for the dissociation than for the association. At each pH (6.5 and 6.8), the difference ΔE_a between the activation energies of dissociation and association was calculated. It was compared with the value of the dissociation free energy determined from the dissociation equilibrium constant measured at equilibrium. At pH 6.5 the value of ΔE_a was 8.9 kcal/mol, $\Delta G°$ determined from the ratio k_{off}/k_{on} was 8.5 kcal/mol, and $\Delta G°$ calculated from the K_D value reported in the literature from equilibrium experiments was 8.7 kcal/mol (*17*). These three values are in close agreement, which provided additional support for a two-state model without intermediate. At pH 6.8, the comparison could not be made since no equilibrium constant has been reported from equilibrium studies at this pH. However, comparing the activation energies at pH 6.5 and 6.8 showed that a small increase of the pH (0.3 pH unit) corresponds to a significant change in the transition state energy, mainly for the dissociation reaction, which suggests that the protonation of the histidine residue, buried in the tetrameric structure, may become the rate-limiting step when the proton concentration decreases.

The dissociation enthalpies ($\Delta H°$) were determined at pH 6.5 and 6.8 from the temperature dependence of the dissociation equilibrium constant estimated from the ratio of the rate constants (data not shown). The dissociation enthalpies $\Delta H°$ were obtained from the slopes of the van't Hoff plot, and the dissociation entropies ($\Delta S°$) were calculated from the values of $\Delta H°$ and $\Delta G°$. For both pHs, positive values of $\Delta H°$ were obtained, and $\Delta S°$ was close to 0 kcal·mol^{-1}·K^{-1}, indicating that the enthalpy constitutes the major energetic component of the dissociation equilibrium. This indicates that the tetramer is destabilized with increasing temperature and that the predominant interactions involved in the association are of enthalpic character. The low entropy component is in agreement with the limited number of hydrophobic contacts seen at the dimer−dimer interface in the 3D structure of the tetramer and with a large contribution of hydrophilic/electrostatic interactions in the oligomerization process.

Identification of Two Phases in the Dissociation Kinetics. In the case of dissociation reactions (Figure 2A), we observed that the first measurable fluorescence intensity was significantly below the fluorescence of the tetrameric protein at pH 8.0, indicating that a decrease of fluorescence occurred during the 4 ms dead time of the stopped-flow machine. Moreover, a careful examination of dissociation kinetics, performed at final pHs around neutrality and low temperatures, showed that the fluorescence first decreased over a time range of about 1 s and then slowly increased to finally reach the equilibrium value. Figure 5 presents such an experiment made at pH 6.8 and at 12 °C. Rather than obeying apparently monophasic kinetics as seen at lower pHs, the reaction was clearly multiphasic. The fluorescence decrease probably corresponded to the end of the "burst" phase seen at lower final pHs. Attempts to fit these kinetics with models involving two, three, or four simple exponentials provided unacceptable results, with high X^2 values and nonrandom distributions of residuals, strongly suggesting that a multimolecular step (presumably the association−dissociation reaction itself) was involved in the fluorescence change. Furthermore, visual comparison of the traces obtained at different pHs (final pH between 6.5 and 7.0) and temperatures (between 12 and 32 °C) indicated that the amplitude of the first kinetic phase increased with increasing the final

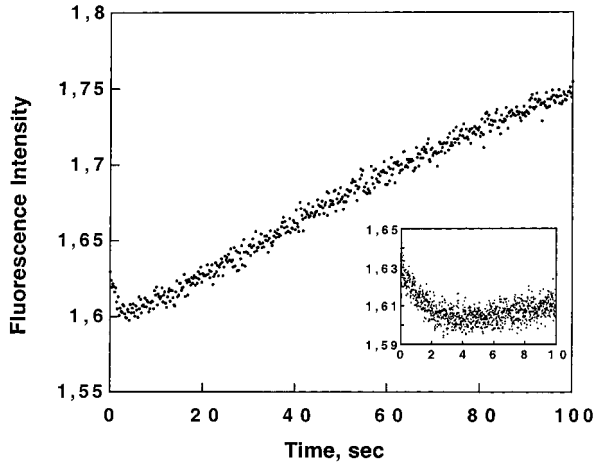

FIGURE 5: Dissociation stopped-flow kinetic trace at pH 6.8 and 12 °C. 20 μL (from the small syringe) of 400 μg/mL R67 DHFR in MTA buffer, pH 8.0, was mixed in 75 ms with 220 μL of MTA buffer, pH 8.0 (from one large syringe), and 180 μL of MTA buffer, pH 5.0 (from the second large syringe). Recording of the fluorescence was triggered at the end of the injection for a duration of 100 s with a sampling interval of 100 ms on one channel and for 10 s with a sampling interval of 10 ms on a second channel (see inset). For both recordings, the filtering constant was 10 ms. All of the experiment was performed at 12 °C, and the number of kinetics accumulated was 10.

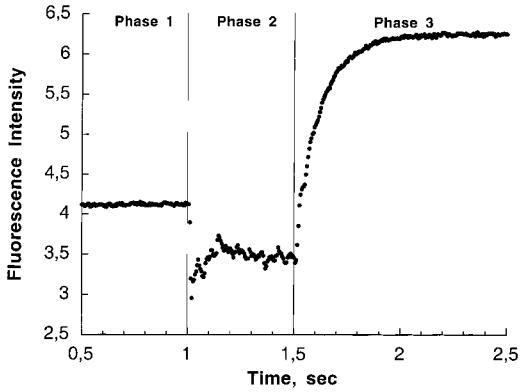

FIGURE 6: Combined fluorescence continuous/stopped-flow analysis of the tetramer dissociation. 20 μL of 400 μg/mL R67 DHFR at pH 8.0 from the small syringe was injected in 70 ms together with 380 μL of MTA buffer, pH 8.0, from the first large syringe, and the flow was interrupted during 500 ms (phase 1). Then, 140 μL of the protein at pH 8.0 from the small syringe and 2.66 mL of MTA buffer at pH 4.5 from the second large syringe were continuously injected during 500 ms (phase 2). The flow was then stopped and the fluorescence recorded in the usual stopped-flow mode during 2 s (phase 3). The temperature was 32 °C. Recording of the fluorescence (λ_{em} above 350 nm) was triggered at the end of the first injection and continued for 2.5 s. The sampling interval and filtering constant were 5 ms. The trace depicted results from the accumulation and averaging of 10 kinetic runs.

pH (up to pH 7.0) and, for a constant pH, with decreasing the temperature. Thus, at pH near 6.8 and 20 °C, a lag rather than a fluorescence decrease preceded the phase of fluorescence increase. Since dissociation is believed to depend on the ionization of His 62, one could imagine that one of these phases might correspond to the protonation step and the second to the dissociation itself. To find out which of the two kinetic phases corresponds respectively to the protonation and the dissociation, dilution experiments at constant pH were performed in order to perturb the association−dissociation equilibrium without changing the ionization state of the preexisting species. This was done at 20 °C by stopped-flow mixing of 20 μL of the protein **(**500 μg/mL**)** previously dialyzed against MTA buffer, pH 6.8, with 780 μL of the same buffer (thus diluting the protein 40-fold) and monitoring the resulting fluorescence change. The kinetics obtained (not shown) showed no burst phase and only a fluorescence increase, indicative of dissociation, with no initial detectable fluorescence lag or decrease during the early reaction times. This suggested that the rapid initial fluorescence decrease observed in downward pH jumps (Figure 5) corresponded to a protonation reaction. Furthermore, the kinetics of fluorescence increase observed after the dilution at constant pH could by no means be fitted with a single exponential, which ruled out that this reaction might be a pseudo-first-order reaction. Since a protonation reaction should obey pseudo-first-order kinetics, the phase of fluorescence increase could not correspond to a simple protonation step. Moreover, the slow fluorescence increase could be well fitted with a reversible, two-state association−dissociation model using the same procedure as that described under Materials and Methods to process the pH jump experiments. These results strongly suggested that the rapid phase of fluorescence decrease observed in pH jumps corresponds to the protonation and demonstrated that the slow phase of fluorescence increase reflects the oligomerization change.

Attribution of the Fluorescence Signals to the Different Molecular Species. (A) Fluorescence Properties of the Dimer. According to a previously proposed model (*17*), protonation of the dimers would be the triggering event in the dissociation, and the pH dependence of the tetramerization would result only from the protonation of the dimers which would remove them from the equilibrium, thus leading to a readjustment of the association−dissociation equilibrium. It therefore could be envisaged that the pH might affect the fluorescence of the dimer and that the rapid fluorescence decrease observed in pH jumps (Figure 5) might correspond to the protonation of preexisting dimer. To test this possibility, we have used a R67 DHFR mutant (S59A) in which both tryptophan 38 and histidine 62 are preserved but which, though folded into a stable dimer, is unable to associate into tetramers whatever the pH (*14*). As shown in Figure 1, the fluorescence spectra of this mutant at pH 8.0 and 5.0 are identical and indistinguishable from that of the protonated wild-type dimer. This indicates that the pH does not affect the fluorescence of the dimer, rules out that the rapid phase of fluorescence decrease might correspond to the protonation of preexisting dimers, and clearly indicates that this rapid phase must reflect a change that occurs within the tetramer when (or after) it becomes protonated but before it dissociates.

(B) Fluorescence Properties of the Protonated Tetramer. The specific fluorescence of the protonated tetramer was determined using the following rationale. By performing a pH jump from 8.0 to a low pH (i.e., high proton concentration) and high (but not denaturing) temperature, one should render the protonation phase extremely fast and ascertain that the initial fluorescence decrease is completed during the dead time of the stopped-flow machine. In such an experiment, the fluorescence observed immediately after the dead time, i.e., before significant dissociation has occurred, should therefore correspond to that of the protonated tetramer. A combined continuous/stopped-flow experiment was therefore

conducted in which a pH jump from 8.0 to 4.5 was achieved at 32 °C. Figure 6 shows a typical complete fluorescence recording (1000 data points on 5 s) obtained from such an experiment. During the continuous-flow phase, the observation cell was constantly supplied with fresh protein that had resided at pH 4.5 during 4 ms (the dead time of the stopped flow). The average of the 100 fluorescence data points collected during the 500 ms of continuous flow (Figure 6, phase 2) therefore provided a reliable value of the fluorescence intensity of the protonated tetramer, which represents about 80% of the fluorescence of the protein at pH 8.0 (Figure 6, phase 1). However, from the K_D value at pH 8.0 and at the protein concentration used in our stopped-flow experiments, tetramers represent only about 85% of the total protein population at pH 8.0. Thus, the quenching of the tetramer fluorescence due to protonation would represent about 25% of the fluorescence of the unprotonated tetramer. Though a reliable analysis of the amplitude of the burst phase observed in simple stopped-flow experiments (such as shown in Figure 2) could not be made because of its small amplitude, it was clear that, even at pHs in the range of 6.0−6.5, the relative amplitude of the burst was much smaller than that determined at pH 4.5 (Figure 6). This indicated that the pK_a of the group involved in this burst phase was below pH 6.5, which suggested that it might indeed be the buried histidine 62.

To further ascertain this conclusion, the fluorescence of the double mutant (S59A, H62L) of R67 DHFR was investigated. This mutant bearing simultaneously the S59A and H62L mutations, constructed and studied in the laboratory (*14*), was shown to form a tetramer with a dissociation constant ($K_D = 2.2$ μM) which, though slightly higher than that of the wild-type enzyme, does not depend on the pH. Furthermore, this double mutant is fully active, indicating that neither its tertiary nor is its quaternary structure affected by the mutations. Thus, if the fluorescence quenching that occurs in the wild-type tetramer is indeed due to histidine 62, it should not be visible in the double mutant. If, on the contrary, it results from the protonation of another group, the fluorescence of the double mutant should be quenched at acidic pH. The fluorescence spectrum of the double mutant was therefore recorded at pH 5.0 and 8.0 at a protein concentration (11.5 μM in dimers) 5-fold higher than the dissociation constant of the double mutant, i.e., under conditions where the protein is mostly tetrameric. The spectra at the two pHs (data not shown) were indistinguishable, which confirmed that His 62 was indeed responsible for the pH-induced fluorescence quenching observed in the wild-type tetramer.

DISCUSSION

As a complement to previously reported thermodynamic investigations performed at equilibrium (*14*, *17*), the experiments reported above deal with kinetic aspects of the reactions that control the dimer−tetramer equilibrium in R67 DHFR. They were aimed at refining our understanding, at the atomic level, of the interactions involved in the dimer−dimer interface and, more specifically, of the mechanism by which the pH controls the association−dissociation equilibrium. The results we obtained can be analyzed at two different levels.

Scheme 1

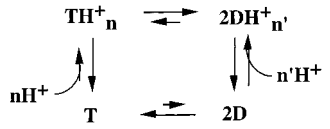

A Simple Two-State Equilibrium: Kinetic and Thermodynamic Approaches. As a first approximation, one can neglect the complex kinetics observed under certain limiting conditions (dissociation at pHs above 6.5 and low temperatures) and consider only those monophasic kinetics that can be globally described according to a simple two-state model, i.e., a one-step association−dissociation reaction involving only the dimers and tetramers regardless of their protonation state. The good quality of the fittings seemed to justify the use of a simple two-state model. This was further supported by the good agreement between the apparent equilibrium dissociation constants obtained from equilibrium studies (*25*) and from the ratio of the apparent dissociation and association rate constants (Figure 3C) and between the free energies of dissociation calculated from these apparent equilibrium constants and from the difference between the activation energies of the association and dissociation reactions. Comparing the standard free energy, enthalpy, and entropy of the dissociation (Table 1) indicates that the basic contribution to the stability of the tetramer is enthalpic, which strongly suggests that hydrophobic interactions are not involved in the association to a significant extent. Moreover, the values of these thermodynamic parameters closely fit with those expected for the contribution of four hydrogen bonds. This, together with the pH dependence of the association and dissociation rate constants and with our observation that all single mutants lacking His 62 fail to associate (*14*), brings strong support to the idea that the major contributors to the stability of the association are the four hydrogen bonds involving the His 62 residues from the four subunits.

A Four-State Model. However, the simple model used for the above analysis is certainly an oversimplification. It cannot account for the kinetic behavior of the system throughout the ensemble of experimental conditions we used. A more complex model should therefore be imagined on the basis of the following observations.

(i) The fluorescence change triggered by a pH drop shows two phases that shall be named rapid and slow for further discussion.

(ii) The rapid phase reflects a pH-dependent reaction that occurs within the tetramer.

(iii) This reaction is likely the protonation of His 62.

(iv) Once protonated, the tetramer undergoes a readjustment of the association−dissociation equilibrium that apparently obeys a simple two-state model.

(v) The kinetics of association induced by a pH increase are monophasic, correspond to a bimolecular reaction, and suggest that it is predominantly the nonprotonated dimer that undergoes association.

The simplest model that incorporates all of these features and accounts for the observations made throughout the pH range investigated in the present study is depicted in Scheme 1. In this square model, the large horizontal arrows indicate the predominant pathways utilized for each of the dissociation and association reactions. Accordingly, the dissociation involves predominantly the protonated tetramer, while the

association reaction is undergone primarily by the unprotonated dimer. The experimental evidence on which this model is based will now be discussed.

(i) The existence of more than one phase in the dissociation kinetics is clearly visible after a downward pH jump. At final pHs below 6.5, a significant fluorescence drop occurs as a burst during the dead time and is followed by a slower phase of fluorescence increase. This is very clearly seen in combined continuous/stopped-flow experiments (Figure 6). At final pHs of 6.5 or above and at lower temperatures, the burst phase is slowed and results in an observable phase of fluorescence decrease or a lag (Figure 5).

(ii) The rapid phase disappeared in the dissociation experiments at constant pH, indicating that this phase results from a protonation reaction within one of the preexisting species. Moreover, the fluorescence of the dimer is not pH-dependent, as demonstrated with the S59A mutant, which ruled out that the rapid fluorescence decrease might occur in the dimer. Thus the rapid fluorescence decrease can take place only inside tetramers. The experiment depicted in Figure 6 showed that protonation of the tetramer results in a quenching by about 25% of its fluorescence.

(iii) The pH dependence of R67 DHFR fluorescence in the pH range 5.0−8.0 suggests the presence of an ionizable group with a pK_a near 7. Side chains with such a pK_a are likely to be histidine residues (*41*). Moreover, histidines are able to quench tryptophan fluorescence through intramolecular proton transfer reactions. In tetrameric R67 DHFR, the distance between the tryptophanyl residue 38 of each polypeptide chain to the histine 62 that belongs to the symmetry-related protomer is 5.6 Å (*26*). This is close enough to let His 62 residues quench the fluorescence of their neighboring tryptophanyl residues, an effect which is enhanced when the imidazole ring is protonated (*42*, *44*). This much stronger quenching power of protonated histidine as compared to the unprotonated species has already been observed on several proteins (*42*, *45*) and can account well for the decrease of fluorescence intensity observed at early times of dissociation kinetics. Finally, no pH dependence of the fluorescence spectrum could be observed for the double mutant (S59A, H62L), as opposed to the wild type. Because a serine side chain can by no means have a pK_a between 7 and 4.5 (the range where a pH change affects the amplitude of the rapid phase), serine 59 cannot be responsible for the observed effect. It must therefore be the replacement of His 62 by leucine which renders the fluorescence of the tetrameric double mutant insensitive to a pH change. Taken together, these observations leave little doubt that the protonation of His 62 inside preexisting unprotonated tetramers is indeed the direct cause of the fast fluorescence decrease.

(iv) As already pointed out, the slow phase that is observed after the protonation of the tetramer in pH jumps or upon dilution of the protein at constant pH can be nicely simulated using a simple two-state association−dissociation model. Moreover, the pH dependence of the amplitude of this phase closely resembles the previously reported pH dependence studies at equilibrium (*17*). The slow phase thus corresponds to the association−dissociation component of the relaxation of the protein after a pH jump.

(v) Let us now consider the association reaction. All of the observed kinetics looked monophasic without any "burst" phase and could be well simulated using a two-state association−dissociation model by including only a first-order dissociation reaction and a second-order association reaction. Figure 3A clearly indicates that increasing the pH results in an increase of the association rate constant, with half the maximum value of the rate constant reached at around pH 7.0. This value points to the deprotonation of an exposed histidine as the key factor in controlling the rate of association, already suggesting that the dimer with its His 62 side chains unprotonated may be the main reactive species. If the association involved primarily protonated dimers, increasing the pH would reduce the concentration of reactive, protonated dimers, thus reducing the apparent rate constant of the association reaction. Conversely, if the association involved primarily unprotonated dimers, increasing the pH would increase the concentration of reactive unprotonated dimers, thus increasing the apparent rate of association. Obviously, only the latter hypothesis is compatible with our observations (Figure 3A). It therefore can be concluded that the preferred association pathway involves unprotonated dimers.

This set of considerations clearly supports the square model proposed above. Why then could the system be analyzed according to a simple model which did not distinguish the protonated from the unprotonated forms of each species? One should reconsider the rate constants determined by using, in the fitting equations, the total population of tetramers (respectively dimers). For example, the apparent association rate constant k_{on} is defined by equation:

$$\frac{d[T_{tot}]}{dt} = k_{on}[D_{tot}]^2 \qquad (7)$$

where $[D_{tot}]$ and $[T_{tot}]$ are the total concentrations of dimers and tetramers (protonated and unprotonated). Since association involves essentially the unprotonated dimers, the real association rate constant, k_0, is defined by

$$\frac{d[T_{tot}]}{dt} = k_0[D]^2 \qquad (8)$$

where [D] is the concentration of unprotonated dimers. The total concentration of the dimer is

$$[D_{tot}] = [D] + [DH^+] = \frac{[D][H^+]}{K_a} + [D] \qquad (9)$$

where D and DH^+ are dimeric forms of unprotonated and protonated R67 DHFR and K_a is the protonation equilibrium constant of the dimer. Thus, the apparent association rate constant is related to the real association rate constant by the equation:

$$k_{on} = k_0(1 + 10^{pK_a - pH})^{-2} \qquad (10)$$

The solid line in Figure 3A represents the best fit of the data using the expression of k_{on} as a function of pH and gives a pK_a value of 6.6 in agreement with previous equilibrium studies (*17*) and structural observations made by X-ray crystallography showing that His 62 is solvent exposed in the dimer (*18*). In fact, the simple two-state model first seemed reasonable since most of the fluorescence change

reflected the change in oligomerization state and since the kinetics of protonation and deprotonation are expected to be very rapid. Indeed, we demonstrated that the pH had no effect on the fluorescence of dimers (S59A dimeric single mutant) and only a small effect on the fluorescence of the tetramer. In terms of kinetics, the protonation−deprotonation reactions of the exposed His 62 in the dimer are expected to be extremely rapid since the protonation of imidazole in solution is diffusion controlled and has a second-order rate constant around 10^{10} s^{-1}•M^{-1} (*46*, *47*). At pH below 7, the apparent association rate constant would be larger than 10^3 s^{-1}. Similarly, with a pK_a of a solvent-exposed histidine side chain about 6.0, one can estimate its rate constant of deprotonation to be about 10^4 s^{-1}. However, protonation of the imidazole ring can be slowed significantly if the histidine is buried within the core of the protein, as in the tetramer where His 62 is shielded from solvent inside the intersubunit interface (*19*). Yet, though the slight deviation from monophasic kinetics observed for the dissociation at pHs above 6.5 and low temperatures reflects this effect, protonation of the tetramer was completed within less than 4 ms in most experiments. Thus, both the protonation and deprotonation reactions were too fast to elicit detectable kinetic phases, which resulted in apparently simple, monophasic kinetics. Analyzing these kinetics according to a single one-step reversible reaction is equivalent to using the square model in which the protonation−deprotonation of both the dimer and the tetramer is considered as infinitely rapid. However, this analysis leaves several questions open. Is only one protonated histidine residue enough to destabilize the tetramer or should the four histidines be protonated? Evidence collected from the complementation between single mutants at positions 62 and 59 indicates that the formation of two hydrogen bonds per tetramer is sufficient to confer a significant stability to the tetramer (*14*). Thus protonation of all of the His 62 residues of a tetramer may well be not fully cooperative, which would introduce an additional degree of complexity.

In conclusion, the results reported above bring additional detailed information on the mechanisms of the protein−protein interactions involved in the R67 DHFR oligomerization. They confirm that the motor of the dimer−dimer association resides in the establishment of four hydrogen bonds per tetramer. They establish that the pH regulates the equilibrium tetramer−dimer by adjusting the dissociation energy barrier. They demonstrate that protonation of histidine 62 within the tetramer triggers the dissociation. These indications will be of major importance in designing mechanistic models of the pH effects on other pH-dependent oligomers.

ACKNOWLEDGMENT

We thank Dr. Thierry Rose for initial genetic constructs and technical advice in purification, Julie Dam for providing the plasmid corresponding to the S59A mutant, and Dr. Alain Chaffotte for helpful assistance with the Figure P software and kinetic expertise. The stimulating discussions with Dr. A. F. Chaffotte are also gratefully acknowledged.

REFERENCES

1. Conte, L. L., Chothia, C., and Janin, J. (1999) *J. Mol. Biol. 285*, 2177−2198.
2. Janin, J., and Chothia, C. (1990) *J. Biol. Chem. 265*, 16027−16030.
3. Janin, J. (1997) *Proteins 28*, 153−161.
4. Amit, A. G., Mariuzza, R. A., Philipps, S. E., and Poljak, R. J. (1986) *Science 233*, 747−753.
5. Braden, B. C., Souchon, H., Eisele, J. L., Bentley, G. A., Bhat, T. N., Navaza, J., and Poljak, R. J. (1994) *J. Mol. Biol. 243*, 767−773.
6. Ward, S. E., Güssow, D., Griffiths, A. D., Jone, P. T., and Winter, G. (1989) *Nature 341*, 544−546.
7. Hawkins, R. E., Russel, S. J., Baier, M., and Winter, G. (1993) *J. Mol. Biol. 234*, 958−964.
8. England, P., Brégégère, F., and Bedouelle, H. (1997) *Biochemistry 36*, 167−172.
9. England, P., Nageotte, R., Renard, M., Page, A. L., and Bedouelle, H. (1999) *J. Immunol. 162*, 2129−2136.
10. Schreiber, G., and Fersht, A. R. (1993) *Biochemistry 32*, 5145−5150.
11. Buckle, A. M., Schreiber, G., and Fersht, A. R. (1994) *Biochemistry 33*, 8878−8889.
12. Schreiber, G., and Fersht, A. R. (1995) *J. Mol. Biol. 248*, 478−486.
13. Schreiber, G., and Fersht, A. R. (1996) *Nat. Struct. Biol. 3*, 427−431.
14. Dam, J., Rose, T., Goldberg, M. E., and Blondel, A. (2000) *J. Mol. Biol. 302*, 235−250.
15. Pattishall, K. H., Acar, J., Burchall, J. J., Goldstein, F. W., and Harvey, R. J. (1977*) J. Biol. Chem. 252*, 2319−2323.
16. Amyes, S. G. B., and Smith, J. T. (1976) *Eur. J. Biochem. 61*, 597−603.
17. Nichols, R., Weaver, C. D., Eisenstein, E., Blakley, R. L., Appleman, J., Huang, T. H., Huang, F. Y., and Howell, E. E. (1993) *Biochemistry 32*, 1695−1706.
18. Matthews, D. A., Smith, S. L., Baccanari, D. P., Burchall, J. J., Oatley, S. J., and Kraut, J. (1986) *Biochemistry 25*, 4194−4204.
19. Narayana, N., Matthews, D. A., Howell, E. E., and Nguyen-huu, X. (1995) *Nat. Struct. Biol. 2*, 1018−1025.
20. Smith, S. L., Stone, D., Novak, P., Baccanari, D. P., and Burchall, J. J. (1979) *J. Biol. Chem. 254*, 6222−6225.
21. Stone, D., and Smith, S. L. (1979) *J. Biol. Chem. 245*, 6222−6225.
22. Bradrick, T. D., Beechem, J. M., and Howell, E. E. (1996) *Biochemistry 35*, 11414−11424.
23. Park, H., Bradrick, T. D., and Howell, E. E. (1997) *Protein Eng. 10*, 1415−1424.
24. Reece, L. J., Nichols, R., Ogden, R. C., and Howell, E. E. (1991) *Biochemistry 30*, 10895−10904.
25. Zhuang, P., Eisenstein, E., and Howell, E. E. (1994) *Biochemistry 33*, 4237−4244.
26. Park, H., Zhuang, P., Nichols, R., and Howell, E. E. (1997) *J. Biol. Chem. 272*, 2252−2258.
27. Northup, S. H., and Erickson, H. P. (1992) *Proc. Natl. Acad. Sci. U.S.A. 89*, 3338−3342.
28. Bradrick, T. D., Shattuck, C., Strader, M. B., Wicker, C., Eisenstein, E., and Howell, E. E. (1996) *J. Biol. Chem. 271*, 28031−28037.
29. West, F. W., Seo, H., Bradrick, T. D., and Howell, E. E. (2000) *Biochemistry 39*, 3678−3689.
30. Martinez, M. A., Pezo, V., Marliere, P., and Wain-Hobson, S. (1996) *Embo J. 15*, 1203−1210.
31. Schagger, H., and von Jagow, G. (1987) *Anal. Biochem. 166*, 368−379.
32. Hillcoat, B. L., Nixon, P. F., and Blackey, R. L. (1967*) Anal. Biochem. 21*, 178−189.
33. Brito, R. M., Reddick, R., Bennett, G. N., Rudolph, F. B., and Rosevear, P. R. (1990) *Biochemistry 29*, 9825−9831.
34. Ellis, K. J., and Morrison, J. F. (1982) *Methods Enzymol. 87*, 405−426.
35. Plesniak, L. A., Connelly, G. P., Wakarchuk, W. W., and McIntosh, L. P. (1996) *Protein Sci. 5*, 2319−2328.
36. Connelly, G. P., and McIntosh, L. P. (1998) *Biochemistry 37*, 1810−1818.

37. Garrett, D. S., Seok, Y. J., Peterkofsky, A., Clore, G. M., and Gronenborn, A. M. (1998) *Protein Sci. 7*, 789−793.
38. Loewenthal, R., Sancho, J., and Fersht, A. R. (1992) *J. Mol. Biol. 224*, 759−770.
39. Zhuang, P., Yin, M., Holland, J. C., Peterson, C. B., and Howell, E. E. (1993) *J. Biol. Chem. 268*, 22672−22679.
40. Xu, D., Tsai, C. J., and Nussinov, R. (1997) *Protein Eng. 10*, 999−1012.
41. Yu, H. T., Colucci, W. J., McLaughlin, M. L., and Barkley, M. D. (1992) *J. Am. Chem. Soc. 114*, 8449−8454.
42. Shinitzky, M., and Goldman, R. (1967) *Eur. J. Biochem. 3*, 139−144.
43. Van Gilst, M., and Hudson, B. S. (1996) *Biophys. Chem. 63*, 17−25.
44. Chen, Y., and Barkley, M. D. (1998) *Biochemistry 37*, 9976−9982.
45. Loewenthal, R., Sancho, J., and Fersht, A. R. (1991) *Biochemistry 30*, 6775−6779.
46. Eigen, M., Hammes, G. G., and Kustin, K. (1960) *J. Am. Chem. Soc. 82*, 3482−3483.
47. Eigen, M., and Hammes, G. G. (1963) *Adv. Enzymol. 25*, 1−38.
48. Smith, S., and Burchall, J. J. (1983) *Proc. Natl. Acad. Sci. U.S.A. 80*, 4619−4623.

BI010611J